

Chapter 2

Experimental Details

Abstract

This chapter describes a detail account of structure, properties and utilities of the polymers which were used in the present work. The preparation of polymer films and organometallics complex and their polymer composite films, estimation of range and energy using SRIM Code, irradiation parameters and detail information about the dose used is also given. The specific details about the techniques used in the characterization of samples are also discussed.

2.0 Introduction

This chapter deals with brief description of the polymeric materials used in the present study and equipments with their relevant details and various techniques for the offline measurements employed in this thesis. The present work gives the description about the following:

1. The Materials: the polymers/polymer composites used and their chemical structure.
2. Irradiation of polymers using 15 MV Pelletron Accelerator at Inter University Accelerator Center (IUAC) New Delhi, India.
3. Sample and Target Preparation, Thickness Measurement and Calculation of Range and Energy Loss by SRIM- Code
4. AC Electrical Frequency Response
5. Vickers's Microhardness
6. Atomic Force Microscopy (AFM)
7. Scanning Electron Microscope (SEM)
8. X-Ray Diffraction (XRD) Study
9. Fourier Transform Infra-Red (FTIR) Spectroscopy
10. Thermogravimetric Analysis (TGA)
11. Differential Scanning Calorimetry (DSC)
12. Mossbauer Spectroscopy

2.1 The Materials

The materials used in the present study are

- (i) Polymethyl methacrylate (PMMA)
- (ii) Polyvinyl chloride (PVC)
- (iii) Polyimide (PI)/Kapton
- (iv) Polycarbonate (PC)/Makrofol-DE
- (v) Polyether sulfone (PES)
- (vi) Polyvinyl chloride (PVC) and Polyethelene terephthlate (PET) Blend Polymer

2.1 (i) Polymethyl methacrylate (PMMA)

Polymethyl methacrylate (PMMA) is an amorphous, transparent and colourless thermoplastic that is hard and stiff but brittle. It has good abrasion and UV resistance and excellent optical clarity [1,2].

Typical Applications

Optics: Dust covers for hi-fi equipment, sunglasses, watch glasses, lenses, magnifying glasses.

Vehicles: Rear lights, indicators, tachometer covers, warning triangles.

Electrical engineering: Lamp covers, switch parts, dials, control buttons.

Office equipment: Writting and drawing instruments, pens.

Medicine: Packaging for tablets, pills, capsules, suppositories, urine containers, sterilisable equipment.

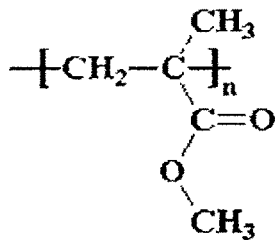
Others: Leaflet dispensers, shatter-resistant glazing, shower cubicles, transparent pipelines, illuminated signs, toys

Physical Properties

Composition



Structure of Polymethyl methacrylate (PMMA)



Density 1.17 g/cm³

Glass Transition Temperature 105 °C

Melting Temperature 130-140 °C

Heat Deflection Temperature <100 °C

2.1 (ii) Polyvinyl Chloride (PVC)

Polyvinyl chloride (PVC) is an important polymer used extensively. Its molecular formula is $[-(-CH_2 -CHCl)-]_n$. Polyvinylchloride (PVC) is one of the most important polymers currently used worldwide. This is because PVC is one of the cheapest polymers to make and has a large range of properties so can be used to make hundreds of products [1].

PVC is formed by the polymerisation of vinyl chloride (chloroethane) monomer units. Polymerization of vinyl chloride, $\text{CH}_2=\text{CHCl}$ (chloroethene), produces a polymer similar to polyethylene, but having chlorine atoms at alternate carbon atoms on the chain.

The vinyl chloride polymers are mainly amorphous thermoplastics with very good chemical resistance. PVC is the most widely used member of the vinyl family. On every other carbon in the backbone chain, one of the hydrogen atoms is replaced with a chlorine atom. It is produced by the free radical polymerization of vinyl chloride. Resins of polyvinyl chloride are hard, but with the addition of plasticizers a flexible, elastic plastic can be made.

Polyvinyl chloride (PVC) is rigid and somewhat brittle. PVC has a good chemical resistance, especially against oils. It has a high strength-to-weight ratio and is a good electrical and thermal insulator. PVC is also self-extinguishing per UL flammability tests. PVC may be used to temperatures of 140°F (60°C) and is readily available in sheets, rods, and tubing. PVC may be cemented, welded, machined, bent and shaped readily. It is water resistant. It has flame resistance, too, because it contains chlorine.

PVC consists of polar molecules attracted to each other by dipole-dipole interactions due to electrostatic attractions of a chlorine atom in one molecule to a hydrogen atom in another atom. These considerable intermolecular attractions between polymer chains make PVC a fairly strong material. Uncompounded PVC is colourless and rigid and possesses poor stability towards heat and light.

About two-thirds of the PVC produced annually is used in the manufacture of pipes and fittings. It is also used in the production of "vinyl" sidings for houses and clear plastic bottles.

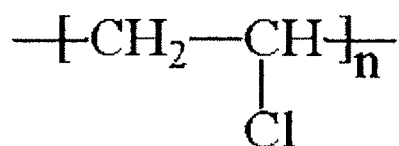
When it is blended with a plasticizer such as a phthalate ester, PVC becomes pliable and is used to form flexible articles such as raincoats and shower curtains. Their combination with plasticizer opens up many useful applications, ranging from artificial leather to injection molding components. This plastic has found extensive use in the manufacture of wires and cables. Cloth and paper can be coated with it to produce fabrics that may be used for upholstery materials and raincoats [3,4].

Physical Properties

Composition



Structure of Polyvinyl chloride (PVC)



Density 1.380 g/cm³

Glass Transition Temperature 87 °C

Melting Temperature 212 °C

Heat Deflection Temperature 100 °C

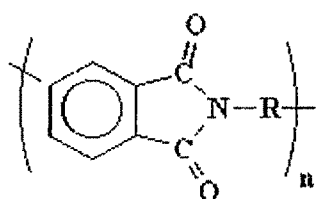
2.1 (iii) Polyimide (PI) / Kapton

Polyimides represent an important class of high-temperature, solvent-resistant polymers. Often, polyimides are formed by a two stage process. The first step involves the polycondensation of an aromatic dianhydride and aromatic diamine to form an intermediate poly(amic acid). Dehydration of the poly(amic acid) at elevated

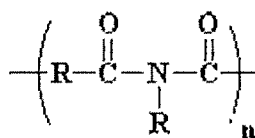
temperatures yields the polyimide (PI) structure. Unlike the intermediate poly(amic acid), the cured (i.e. fully imidized) PI is insoluble and infusible and has high temperature and oxidative stability and good electrical insulation properties and radiation resistance. Commercially important PI is a polypyromellitimide that is available as film is Kapton.

Kapton is one of the heat resistive and most technologically important polymer which has attracted the attention of scientists and material engineers since the last few decades. It has wide applications in different technologies especially in nuclear and satellite fabrication technology. It has sufficient U.T.S. and its working temperature ranges from liquid Helium temperature to 400°C for continuous use [1].

Polyimide usually are in two forms. The first of these is linear structure where the atoms of the imide group are part of linear chain. The second of these structures is a heterocyclic structure where the imide group is part of cyclic unit in the polymer chain.



aromatic heterocyclic polyimide



linear polyimide

Polyimide is yellow in colour, transparent, soft and is a thermoplastic polymer. It has excellent thermal stability, good dielectric properties and excellent mechanical strength. It can withstand a temperature of 425°C without undergoing any degradation. Kapton has high radiation resistance. Hence it is a suitable polymer for radiation application. It is used in the insulation coating of electromagnetic wirings, surface coatings in supersonic aircraft, backings and windows in many nuclear physics

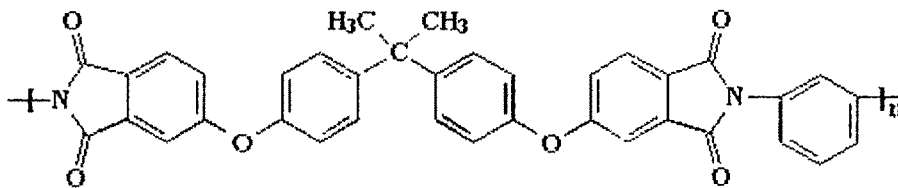
experiments, microfilters, IC fabrication, passivations and multilayer interconnections in microelectronics, etc. Kapton has wide applications in different technologies especially in nuclear and satellite fabrication technology. Typical uses for polyimides include electronics, sleeve bearings, valve seatings and as the matrix component of graphite composites for compressor vanes in jet engines and other aerospace applications [5].

Physical Properties

Composition



Structure of Polyimide



Density 1.42g/cm³

Glass Transition Temperature 385 °C

Melting Temperature >400 °C

Heat Deflection Temperature 360 °C

2.1 (iv) Polycarbonate (PC)/Makrofol-DE

A crystal clear and colorless, amorphous engineering thermoplastic notable for its high impact resistance. It has reasonably good temperature resistance, good dimensional stability and low creep but somewhat limited chemical resistance and is prone to environmental stress cracking [1].

Polycarbonate is a clear plastic, used to make shatterproof windows, lightweight eye glass lenses. Polycarbonate gets its name from carbonate groups, in its backbone chain.

There is a fundamental difference in the two types of PC. One is polycarbonate of bisphenol A, is made from bisphenol A and phosgene. Polycarbonate bisphenol A is thermoplastic.

The other polycarbonate can make up by allyl groups. These allyl groups have carbon- carbon double bonds in them. It can polymerize by free radical vinyl polymerization. The two allyl groups will become parts of different polymer chains. The carbonate containing groups for the cross links between the polymer chains. This cross linking is making the material very strong. This polycarbonate is thermoset.

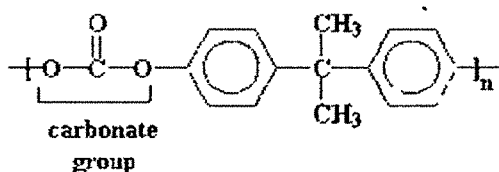
Applications include glazing, safety shields, lenses, eyeglasses, casings and housings., light fittings, kitchenware (microwaveable), medical apparatus (sterillisable) and Cd's (the disc).

Physical Properties

Composition



Structure of Polycarbonate



Density 1.2g/cm³

Glass Transition Temperature 150 °C

Melting Temperature 265 °C

Heat Deflection Temperature 128-138 °C

2.1 (v) Polyether sulfone (PES)

An amorphous, transparent and pale amber high performance thermoplastic with the common characteristics of Polyether ether ketone (PEEK). Polyether sulfone/PES is high performance polymers. It acts more like polycarbonate, but PES is much more heat resistant, It can stand up well to water and steam, so they are used to make things like cookware and medical products that need to be sterilized between uses [1,2].

PES gets their name because they have ether groups and sulfone groups in their backbone chains. It has relatively high water absorption and, in common with many other plastics, drying is essential before e.g. thermoforming. It has poor fatigue characteristics and is prone to environmental stress cracking but has good long term thermal ageing resistance and reasonable radiation resistance. Its chemical resistance is not as wide as PEEK's; hence solutions can be made if solvents are correctly chosen.

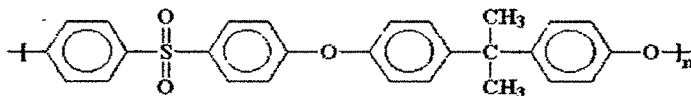
Applications include electrical and electronic components, medical etc. Equipment that needs repeated sterilization and photographic accessories.

Physical Properties

Composition



Structure of Polyether sulfone



Density 1.37g/cm³

Glass Transition Temperature 225 °C

Melting Temperature >400 °C

Heat Deflection Temperature 203 °C

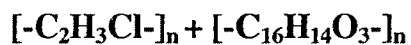
2.1 (vi) Polyvinyl chloride (PVC) and polyethelene terephthlate (PET)

Blend Polymer

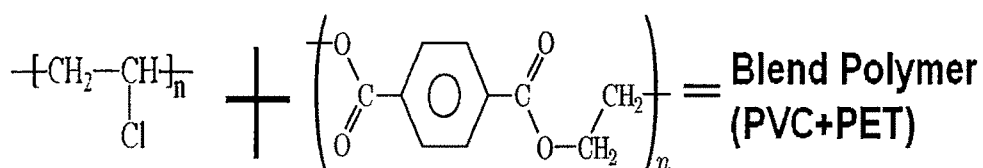
This polymer was prepared in the laboratory in equal proportion of PVC (IPCL made) with commercial grade PET (Garware made) in two roll mill. The PVC and PET were taken in granuals form and in pure form too (wt/wt). The mixture was transformed into sheet at around 125 °C for half an hour.

Physical Properties

Composition



Structure of polymer blend



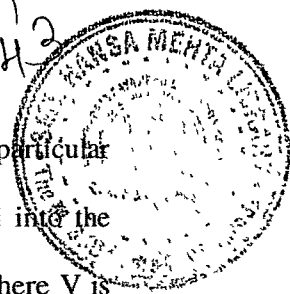
	PVC	PET
Density (g/cm ³)	1.380	1.3-1.4
Glass Transition Temperature	87 °C	69 °C
Melting Temperature	212 °C	265 °C
Heat Deflection Temperature	100 °C	80 °C

2.2 Pelletron Accelerator

15 UD Pelletron accelerator at Inter University Accelerator Center (IUAC) New Delhi [6] belongs to a class of particle accelerator known as Van de Graff electrostatic accelerator. It is capable of accelerating any ion from proton to uranium (except the inert gases) in the energy range from a few tens of MeV to a few hundred MeV, depending on the ion species. The accelerator is installed in vertical geometry in a stainless steel tank which is 26.5 meter high and 5.5 meter diameter. In the middle of the tank, there is a high voltage terminal which can hold potential from 4 to 16 MV. The terminal is connected to the tank vertically with ceramic-titanium accelerating tubes. The tank is filled with a high dielectric constant SF_6 gas at 6-7 atmospheric pressure to insulate the high voltage terminal from the tank wall. A potential gradient is maintained through the accelerating tubes from the ground potential, and from the terminal to the potential, at the bottom of the tank. A schematic diagram of Inter University Accelerator Center (IUAC) pelletron accelerator is shown in Figure 2.1.

In this machine, negative ions are produced and are re-accelerated to 400 KeV, mass analyzed and are then injected into a strong electrical field inside the accelerator. At the center of the accelerator tank there is a terminal shell which is maintained at high voltage (up to 15 million volts). The negative ions on traveling through the accelerating tube from the top of the tank towards the positive terminal and get accelerated. On reaching the terminal, they pass through a stripper that strips the ions of their electrons, thus transforming them to positive ions. These positive ions are repelled from the terminal (due to positive potential) and thus are again accelerated to ground potential to the bottom of the accelerator, i. e. the same terminal potential is used twice to accelerate

P/Th
11/11/2



the ions. After exit from the accelerator, the ion beam corresponding to a particular energy is selected and bent by an analyzing magnet. Negative ions injected into the accelerator column are accelerated to the terminal and gain energy V MeV, where V is the terminal potential. The terminal has a foil stripper assembly (thin carbon foil) as well as a gas stripper (nitrogen gas at low pressure). As the ions pass through the stripper, they strip off some of the electron to become positive ions. Depending on the foil thickness (or gas pressure), the incident energy and type of the ions, the charge state distribution of the emerging positive ions will vary. The most probable charge state and other states after stripping can be calculated by semi-empirical formula. These ions are further accelerated while traveling to high energy end of the accelerator and gain energy equal to qV , where q is the charge state. As a result the ions emerging out of the accelerator [7] column gain energy given by

$$E_1 = [E_{inj} + (1+q) V] \text{ MeV} \quad (2.1)$$

Where, E_1 the energy of the ion having a charge state q after stripping. V is the terminal potential in MV (million volts) and E_{inj} is the energy of injected particle in MeV. The ion beam emerging from the accelerator is focussed at the object point of an analyzing magnet by means of magnetic quadrupole triplet lens placed at the accelerator exit. The pelletron ion beam is generally composed of several components, each with different charge state and energy. However, for the experimental purpose [8] precise monoenergetic ions are required. So the pelletron high energy beam line following the main accelerating tube includes an energy dispersive, homogeneous dipole magnet, which can be so set that all unwanted ion beam components are filtered out leaving only the selected component for onward transmission to the beam lines.

For an ion beam having mass M , energy E , and charge state q , the analyzing field required for selection of such a beam is governed by the relation

$$B = K (ME)^{1/2}/q \quad (2.2)$$

Where K is constant. Setting different magnetic field strength (B), one can choose different M , E and q of the ions. The entire beam transport system of the 15 UD Pelletron accelerator is maintained under a clean ultra high vacuum condition i.e. at pressure below 1×10^{-9} torr. This is achieved by the use of different types of vacuum pumps distributed all along the beam line from the ion source to the irradiation chamber. The ion beam of a desired energy (E) and mass (M) is transported into any one of the seven beam lines of the beam hall by means of a switching magnet. Seven beam lines are shown in Figure 2.2. The beam is kept centered and focused by means of steering magnet. The beam is visually monitored by beam profile monitors and the beam current is measured by means of Faraday cups [6].

High fluence irradiation set up at IUAC

In this setup, high vacuum chamber (38 cm diameter) has a facility for temperature controlled (liquid cooled) multiple sample holders having provision for linear movement of 120 mm and a rotation of 360° . A vacuum of 10^{-7} mbar is maintained by using a diffusion pumping system filled with a LN_2 trap. A remote controlled target holder can be positioned perpendicular to the beam line for irradiation. Various samples can be irradiated in an experiment using below scaled linear movement of the holder by 140 mm. Material science beam line is used for ion fluence up to 10^{14} ions/cm². Figure 2.3 shows the material science irradiation chamber at Inter University Accelerator Center (IUAC), New Delhi. For irradiation we have to see whether beam is falling at the desired

place on the quartz or not, then we allow the beam to fall on the samples. The rectangular ladder used to fix up six samples contains four faces and its position can be changed by auto control switches. ACCTV camera was also attached to one of the ports of chamber for viewing the sample position.

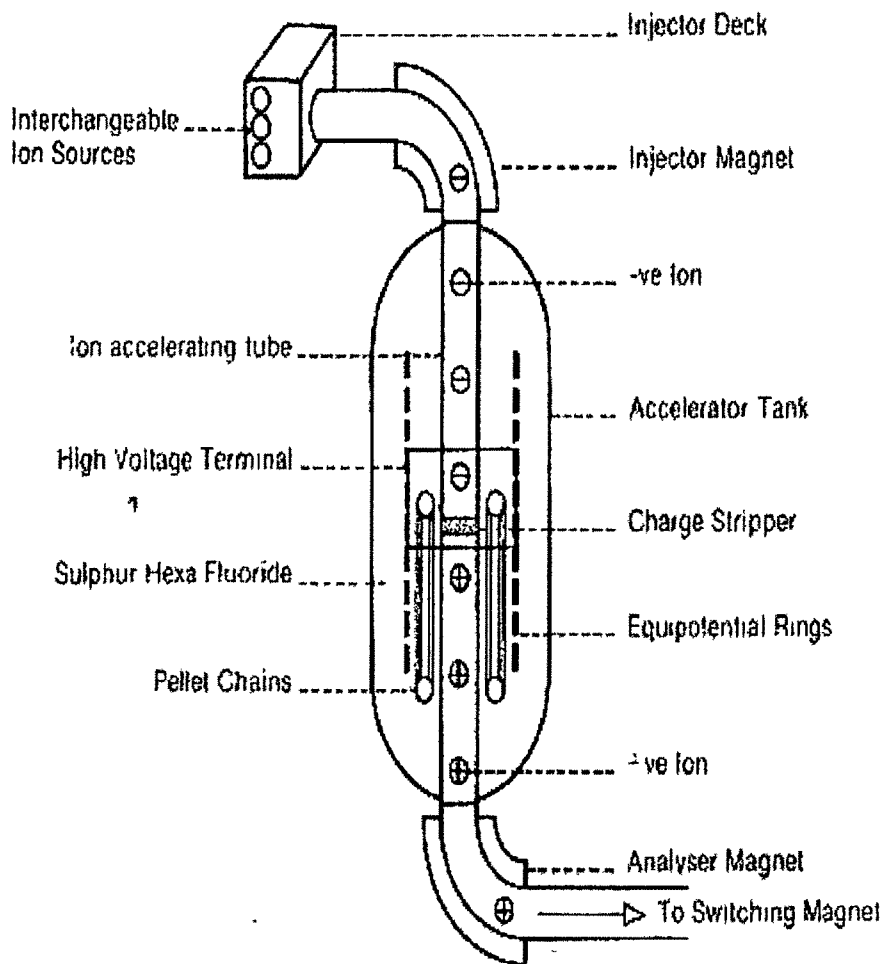


Figure 2.1 Schematic diagram of IUAC Pelletron accelerator.

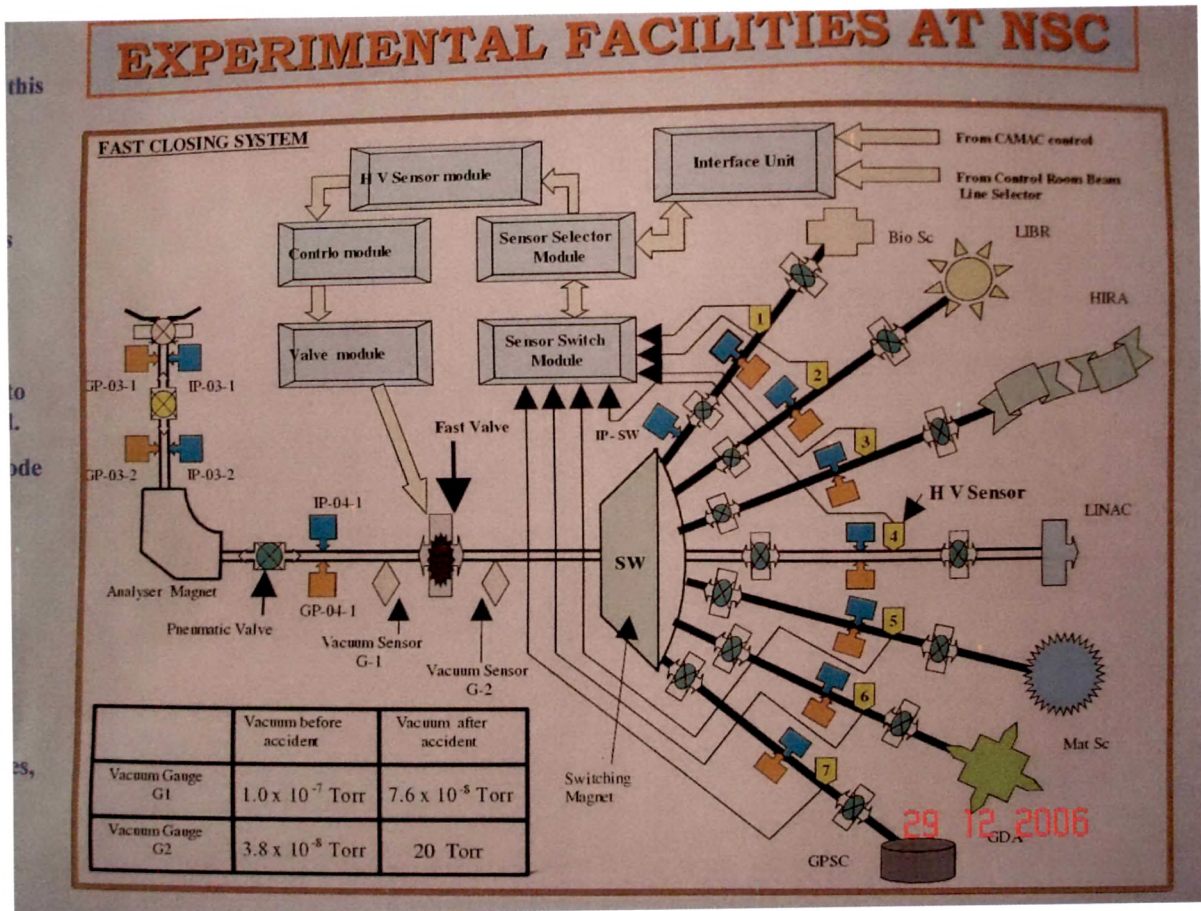


Figure 2.2 Schematic diagram of beam lines at IUAC Pelletron facility.

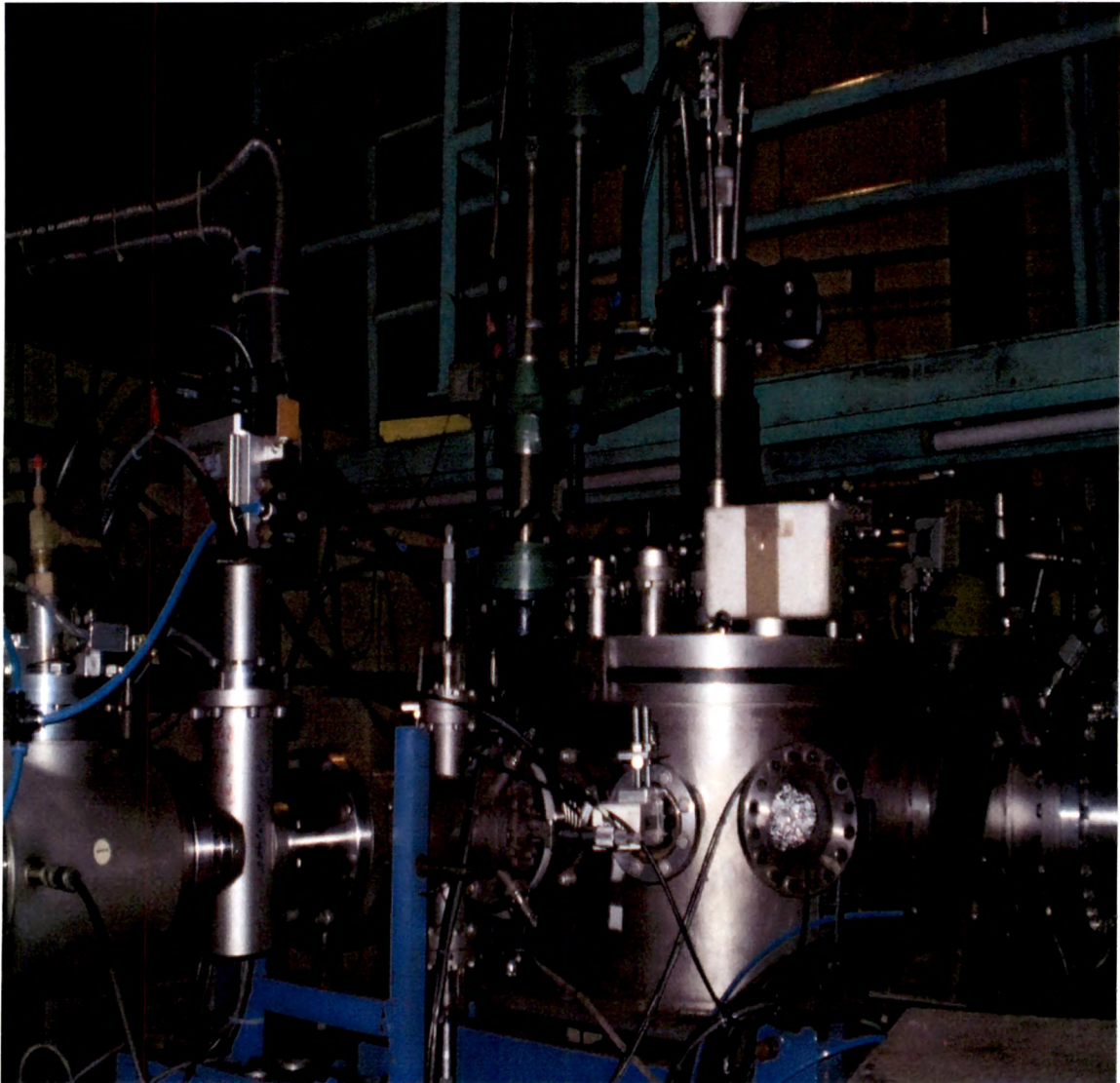


Figure 2.3 Material science irradiation chamber at IUAC Pelletron facility.

2.3 Irradiation and Measurements

2.3.1 Sample and Target Preparation

2.3.1 (i) Preparation of PMMA

PMMA was prepared by solution polymerization method. In this method Benzoyl peroxide (BPO, 0.8g; an initiator for polymerization) were dissolved in freshly inhibitor free MMA (80 ml methyl methacrylate) monomer and ethyl acetate as a solvent (80 ml) in a round bottom flask, the solution was then refluxed for 5h at 80⁰C temperature in the hot water bath. The resulting solution was then precipitated out in another beaker containing methanol (100 ml).The PMMA, precipitated out in methanol, was dried at room temperature for 2 h.

2.3.1 (ii)Preparation of an organometallic compound

As an organometallic compound we took ferric oxalate and Nickel dimethylglyoxime (Ni-DMG).

2.3.1 (ii) (a) Preparation of Ferric oxalate

Ferric oxalate was formed by taking 6.24g of oxalic acid and 5.24g of ferric chloride with ethanol as a solvent in a round bottom flask, and it was refluxed for 4h at 60⁰C. The excess of ethanol was then distilled out and the substance was dried at 75⁰C for 3h in an oven.

2.3.1 (ii) (b) Preparation of Ni-DMG

Nickel dimethylglyoxime (Ni-DMG) was formed by dissolving 0.4 mole nickel chloride in 200 ml water and it was heated at 80⁰C; a slight excess of the alcoholic dimethylglyoxime (DMG) was added and then dilute ammonia solution was added drop

wise with continuous stirring until precipitation took place. The precipitate was then washed with cold water until free from Cl^- and dried at 110°C for 1h.

2.3.1 (iii) Preparation of ferric oxalate and Ni-DMG dispersed PMMA and PVC films

The polymerized PMMA and commercially available PVC powder were mixed with ferric oxalate compound of 5%, 10%, and 15% separately and dissolved using acetone and the solutions were stirred thoroughly for about an hour and poured on clean glass trough. The solvent was evaporated at room temperature ($25^\circ\text{C} + 1^\circ\text{C}$) to get thin films (thickness $\sim 50\mu\text{m}$) of dispersed PMMA with 5%, 10%, and 15% concentration of ferric oxalate compound.

The polymerized PMMA and Ni-DMG compound of 5%, 10%, 15%, 20%, 30% and 40% were dissolved using toluene; acetone (50:40) and Briz-35 surfactant (0.5 at% of polymer) the solutions were mixed and stirred thoroughly for about an hour and then poured into a clean glass trough. The solvent was evaporated at room temperature ($25^\circ\text{C} + 1^\circ\text{C}$) to get thin films of thickness $\sim 50\mu\text{m}$. The films were used for irradiation.

2.3.1 (iv) Preparation of PVC and PET blends

The polymeric blend of PVC (IPCL make,) with commercial grade PET (Garware make) was prepared in the laboratory (ERDA) in equal proportion in a two roll mill, and then pressed in a hydraulic press to convert it into a sheet. PVC and PET were taken in granules form and in pure form too (wt/wt). The mixture was transformed into a sheet at around 125°C for half an hour.

Two roll mill (Figure 2.4) consists of a main rotor and a main gear which is connected with the other two gears moving in opposite directions. This gear is attached to

the two rotors having a smooth surface and both heated by electrical filament. After half an hour, the sheet was cooled on the rotor. The sheet was removed from the rotor as soon as the temperature comes down to ambient temperature. Each sheet was cooled further for 7/8 hours and then taken for the study.

Other polymers are available commercially from Good Fellow corporation, UK (polyimide and polycarbonate) and Gharda Chemicals, Bharuch India (polyether sulfone).

Four/five pieces of PI, PC, PES, blended PVC and PET of size 1.5 x 1.5 cm² were cut from the sheets. These were washed thoroughly by soap solution and deionised water. The cleaned samples were then dried inside a vacuum desiccator.



Figure 2.4 Picture of Two roll mill.

2.3.2 Thickness Measurement of Samples

The thickness of these polymers was measured by a sensitive digital instrument. Sensitivity of the instrument was 0.001mm. The thickness of the polymers was measured at 6-7 places chosen randomly and average value was calculated. The measured thickness of samples is listed in **Table 2.1**

Table 2.1: Thickness of the polymers.

Polymer	Thickness
PMMA /Ferric oxalate/Ni DMG composite films	50µm
PMMA /Ni DMG composite films	50µm
PVC / ferric oxalate composite film	50µm
Polyimide (PI)	70µm
Polycarbonate (PC)	413 µm
Polyether Sulfone (PES)	70µm
Blended Polymer (PVC + PET)	460µm

2.3.3 Ion Irradiation

Three / Four pieces of each polymer of size 1.5x1.5 cm² were cut from the sheet. These samples were mounted on a vertical vacuum shielded sliding ladder and irradiated in a material science beam line by using 80 MeV O⁶⁺ ion and 120 MeV Ni¹⁰⁺

ion beams available from a 15UD Pelletron at the Inter University Accelerator Center (IUAC), New Delhi. The irradiation was made at different fluences ranging from 10^{11} to 10^{13} ions/cm². The beam current was maintained around 12 nA in order to avoid excessive heating. The residual pressure in the target chamber was 10^{-6} Torr. The irradiated samples were stored at ambient temperature in air. The details are listed in

Table 2.2

Table 2.2: Details of the irradiation of the polymers

Sr. No	Sample (polymer)	Fluence (ions/cm ²)	Current density nA/cm ²	Energy and Ions
1.	Pure PMMA film	1.0×10^{11}	12	80MeV O ⁶⁺
	PMMA+5%ferric oxalate dispersed film	1.0×10^{11}	12	80 MeV O ⁶⁺
	PMMA+10%ferric oxalate dispersed film	1.0×10^{11}	12	80 MeV O ⁶⁺
	PMMA+15%ferric oxalate dispersed film	1.0×10^{11}	12	80MeV O ⁶⁺
2.	PMMA+5% Ni-DMG dispersed film	1.0×10^{11}	12	80 MeV O ⁶⁺
	PMMA+10%Ni-DMG dispersed film	1.0×10^{11}	12	80 MeV O ⁶⁺
	PMMA+15%Ni-DMG dispersed film	1.0×10^{11}	12	80 MeV O ⁶⁺

3.	Pure PVC film	$1.0 \times 10^{11}, 1.0 \times 10^{12}$	12	80 MeV O^{6+}
	PVC+5% ferric oxalate dispersed film	$1.0 \times 10^{11}, 1.0 \times 10^{12}$	12	80 MeV O^{6+}
	PVC+10% ferric oxalate dispersed film	$1.0 \times 10^{11}, 1.0 \times 10^{12}$	12	80 MeV O^{6+}
	PVC+15% ferric oxalate dispersed film	$1.0 \times 10^{11}, 1.0 \times 10^{12}$	12	80 MeV O^{6+}
4.	Pure PMMA film	$1.0 \times 10^{11}, 1.0 \times 10^{12}$	12	120 MeV Ni^{10+}
	PMMA+5% Ni-DMG dispersed film	$1.0 \times 10^{11}, 1.0 \times 10^{12}$	12	120 MeV Ni^{10+}
	PMMA+20% Ni-DMG dispersed film	$1.0 \times 10^{11}, 1.0 \times 10^{12}$	12	120 MeV Ni^{10+}
	PMMA+40% Ni-DMG dispersed film	$1.0 \times 10^{11}, 1.0 \times 10^{12}$	12	120 MeV Ni^{10+}
5.	Polyimide (PI)	8.5×10^{12}	12	80 MeV O^{6+}
	Polyimide (PI)	1.5×10^{13}	12	80 MeV O^{6+}
	Polyimide (PI)	2.5×10^{13}	12	80 MeV O^{6+}
6.	Polycarbonate (PC)	7.40×10^{12}	12	80 MeV O^{6+}
	Polycarbonate (PC)	1.2×10^{13}	12	80 MeV O^{6+}
	Polycarbonate (PC)	2.4×10^{13}	12	80 MeV O^{6+}
7.	Polyether Sulfone (PES)	6.0×10^{12}	12	80 MeV O^{6+}

	Polyether Sulfone (PES)	1.8×10^{13}	12	80 MeV O ⁶⁺
	Polyether Sulfone (PES)	3.6×10^{13}	12	80 MeV O ⁶⁺
8.	PVC+PET blend	6.0×10^{12}	12	80 MeV O ⁶⁺
	PVC+PET blend	1.8×10^{13}	12	80 MeV O ⁶⁺
	PVC+PET blend	3.6×10^{13}	12	80 MeV O ⁶⁺

2.3.4 Calculation of Rangé and Energy loss using SRIM Code

The interaction mechanisms of ion beam with polymeric materials are discussed in the article 1.5 of Chapter 1.

SRIM consists of a number of computer programmes. This program is used to calculate the stopping and range of ions (10 eV – 2 GeV / amu) into a matter giving a quantum mechanical treatment to the ion-atom collisions. The calculation is made very efficient by the use of statistical algorithms which allows the ion to jump between calculated collisions and then averaging the collision results over the intervening gap.

During the collisions, the ion and atom have a screened Coulomb collision, including exchange and correlation interactions between the overlapping electron shells. The ion has long range interactions creating electron excitations and plasmons within the target. These are described by including a description of the target's collective electronic structure and interatomic bond structure when the calculation is setup (tables of nominal values are given). The charge state of the ion within the target is described using the concept of effective charge, which included a velocity dependent charge state and long range screening due to the collective electron sea of the target.

The particle's energy is reduced after each free-flight path by the amount of electronic energy loss and then (after the collision) by the so-called nuclear energy loss which is the result of transferring momentum to the target atom in the collision. Each ion's history is terminated either when the energy drops below a pre-specified value or when the particle has moved out of the front or rear surface of the target [9].

TRIM (the Transport of Ions in Matter) is the most comprehensive program, included in SRIM. This computer program is available for targets of several layers of different composition.

The program provides output for one and two dimensional distributions of ion range, energy deposition, reflection and transmission characteristics of planar targets, ion's energy loss, target damage, sputtering, ionization, and phonon production. In practical applications of the TRIM program, e.g. in studying the sputtering yield (recoil atoms of a few eV being knocked out of the surface), the TRIM results yield quite satisfactory agreement with the experimental data.

At high energies, it is quite efficient as it takes into account the natural increase in free-flight paths; a particle's free-flight path between noticeable collisions is long at high energies and is steadily reduced in the course of slowing down. The TRIM program contains provisions for dealing with very high energies and includes relativistic electronic energy loss and straggling for high energies. For energies below 1 MeV / amu the electronic straggling, however was found to be of little importance for the projected range profiles and is usually neglected. Some kind of electronic straggling at low energies can be introduced however by using the built-in option of treating the electronic energy loss as dependent on the distance of closest approach in the individual collisions.

SRIM code is thus used to calculate the ion distribution and for quick calculation of damage, detailed calculation with full damage cascades, calculation of surface sputtering, Electron/ Neutron/Photon cascades, various ion energy/angle/positions, special multilayer biological targets, stopping power for ions in gases and the stopping of ions in compounds.

In the present work we have calculated the projected range of 80 MeV O⁶⁺ ions and 120 MeV Ni¹⁰⁺ ions in each polymer/composites along with the electronic and nuclear stopping power using latest SRIM code [9].

Results Obtained from SRIM

Projected range of 80 MeV O⁶⁺ ions in each polymer along with the electronic and nuclear stopping power:

In Polymethylmetha acrylate (PMMA), the projected range was calculated to be 94.58 μm, which is 1.89 times the thickness of the sample. The calculations indicate that 99.95 % of energy is lost due to electronic interaction. The electronic stopping power $(dE/dX)_e$ is 5.73 eV/A⁰, where as nuclear stopping power $(dE/dX)_n$ is 3.342 x 10⁻² eV/A⁰.

In Polyvinyl chloride (PVC), the projected range was calculated to be 97.24 μm, which is 1.94 times the thickness of the sample. The calculations indicate that 99.95 % of energy is lost due to electronic interaction. The electronic stopping power $(dE/dX)_e$ is 5.627 eV/A⁰, where as nuclear stopping power $(dE/dX)_n$ is 3.347 x 10⁻² eV/A⁰.

In Polyimide (PI / Kapton) the projected range was calculated to be 88.82 μm, which is 1.26 times the thickness of the sample. The calculations indicate that 99.94 % of energy is lost due to electronic interaction.. The electronic stopping power $(dE/dX)_e$ is 6.252 eV/A⁰, where as nuclear stopping power $(dE/dX)_n$ is 3.471 x 10⁻² eV / A⁰.

In Polycarbonate (PC) the projected range was calculated to be 98.12 μm . The thickness of the sample is 4.2 times larger than the range. The calculations indicate that 99.94 % of energy is lost due to electronic interaction. The electronic stopping power $(dE/dX)_e$ is 5.528 eV/A^0 , where as nuclear stopping power $(dE/dX)_n$ is $3.148 \times 10^{-2} \text{ eV / A}^0$.

In Polyethersulfone (PES), the projected range was calculated to be 98.2 μm , which is 0.71 times the thickness of the sample. The electronic stopping power $(dE/dX)_e$ is 5.528 eV/A^0 , where as nuclear stopping power $(dE/dX)_n$ is $3.148 \times 10^{-2} \text{ eV / A}^0$.

In blend of Polyvinylchloride (PVC) and Polyethylene terephthalate (PET) the projected range was calculated to be 92 μm . The thickness of the sample is 5 times larger than the range. The electronic stopping power $(dE/dX)_e$ is 6.02 eV/A^0 , where as nuclear stopping power $(dE/dX)_n$ is $3.42 \times 10^{-2} \text{ eV/A}^0$.

Projected range of 120 MeV Ni¹⁰⁺ ions in PMMA along with the electronic and nuclear stopping power:

In Polymethylmetha acrylate (PMMA), the projected range was calculated to be 36.88 μm . The electronic stopping power $(dE/dX)_e$ is $4.267 \times 10^3 \text{ eV/A}^0$, where as nuclear stopping power $(dE/dX)_n$ is 6.070 eV/A^0 .

2.4 Characterization of Polymers

The characterization of the pristine and irradiated samples were done by different techniques viz Fourier transform IR spectroscopy, Scanning electron microscope (SEM), Vickers' microhardness tester, AC electrical frequency response, Atomic force microscopy (AFM), Mossbauer spectroscopy and X-ray diffraction (XRD). The

characterization techniques, instrumental set up and the experimental conditions are described below.

2.4.1 AC Electrical Properties

Many polymeric materials have been very successful in electrical applications because of one or more outstanding properties, such as dielectric strength, volume and surface resistivity, dielectric constant, loss factor and dissipation factor. Crystallinity can affect the dielectric constant. Electrical properties are influenced more by dipole asymmetry than by the presence of polar groups. Polytetrafluoroethylene, for example has a lower dissipation factor than Polyvinyl fluoride; the latter possesses a great dipole asymmetry than the former.

When the dipoles are able to respond readily to change in the electric field (low frequency or high temperature) the dielectric constant is high. At high and low frequencies, the dipoles can either respond completely or not at all to the change in field, and the loss factor which is the product of dielectric constant and power factor is low. The power factor is the sine of the angle of phase difference due to the delay in movement of the dipole with the change in the field.

Although the various types of radiation interact with matter in different ways, the primary process is the production of ions and electrically excited states of molecules which in turn, may lead to the formulation of free radicals, radiation generated mobile electrons, which become trapped at sites of low potential energy. The first phenomenon leads to permanent chemical, mechanical and electrical changes in the materials, while the second results in temporary electrical changes in performance [10]

In polymeric materials, the formation of the free radicals during irradiation leads to scission and cross-linking process that modify the chemical structure of the insulation, generally leading to deterioration of the mechanical properties. This mechanical deterioration frequently gives rise to significant electrical property changes. However, important electrical property changes sometimes occur before mechanical degradation. The extent of scission and cross-linking processes depends on the absorbed dose, the absorbed dose rate, the material geometry and the environment conditions present during the irradiation. Because the free radicals some times decay slowly, there may also be post irradiation effects.

AC conductivity

The study of electrical conduction is one of the important electrical characteristics of dielectric material required not only for practical applications but also for the interpretation of the various physical phenomena. Electrical conductivity is an elegant experimental tool to probe the structural defects and internal purity of material. The profound changes which occur in physical and chemical nature of a material essentially give information through its conductivity data. Useful information regarding the mobility and generation as well as the movement of lattice defects in hydrogen bonded molecules can also be obtained by studying the electrical conductivity of the material.

Most polymers are good insulators in their unfilled state with materials such as polyethylene, polytetrafluoroethylene and polystyrene being among the best insulators known. The conductivity of a material is given by the basic equation

$$\sigma = qn\mu \quad (2.3)$$

where q is the charge on the carrier, n is the concentration of carriers and μ is the drift mobility of the carriers. n and μ are determined by molecular structure and depend on factors such as temperature and applied field.

Conduction may be either electronic with electrons and holes as carriers or ionic with cations and anion as carriers. In most polymeric materials, it is difficult to detect any electronic conductivity and most of the conductivity that is observed is due to impurity ions such as catalyst residues, dissociable end groups and degradation products. Therefore, the resistivity ρ (reciprocal of conductivity) of a polymeric material may be significantly improved by purification of the polymer. Polyamides, however, do display pronounced ionic conduction at elevated temperature which increases by several orders of magnitude between ambient temperature and 100°C . This is probably due to the dissociation of amide groups to give protons with mobility possibly aided by the hydrogen bonding network.

Inherently conductive polymers such as polyacetylene and polypyrrole are now more widely researched and some commercial applications are being considered. Polymers that are rendered conducting by the incorporation of carbon black or metal particles are widely used [11]

The volume resistivity, ρ_v , of a material is the resistance between opposite faces of a unit cube and is an important material parameter in polymer insulation. The surface resistivity, ρ_s , (the resistance between opposite edges of unit square), may also be of importance. For high resistivity materials, ρ_v be measured as a rectangular or cylindrical block of material with electrodes attached to the ends. The volume resistivity, ρ_v , is given by

$$\rho_v = RA/T \quad (2.4)$$

where R is the measured resistance, A is the cross-sectional area of the electrode and T is the specimen thickness. For low resistivity material, ρ_v , is best measured on a thin disc of polymer with electrodes painted on either side.

The conductivity is calculated as $1/\rho_v$ i.e.

$$\begin{aligned} \sigma_v &= 1/\rho_v \\ \sigma_v &= T/RA \end{aligned} \quad (2.5)$$

The surface resistivity, ρ_s , may be measured using concentric ring electrodes. ρ_s is given by

$$\rho_s = 2\pi R \ln(r_1/r_2) \quad (2.6)$$

Where r_1 and r_2 are the radii of inner and outer electrodes, respectively.

This equation (2.5) has been used to calculate the a.c. conductivity of the polymers at different frequencies.

Dielectric Constant

The dielectric constant is the ratio of the capacitance induced by two metallic plates with an insulator between them to the capacitance of the same plates with air or a vacuum between them. It measures the inefficiency of an insulating material. If the material to be used for strictly insulating purpose, it would be better to have a lower dielectric constant. The dielectric constant of solids can greatly vary in magnitude with variations in their structural properties. Any mechanisms of polarization can proceed in solid bodies. Solid nonpolar dielectrics obey the same regularities as nonpolar liquids and

gases. Mechanisms of polarization in solid dielectrics are discussed in article 1.6 of Chapet 1.

A vacuum capacitor with an electric field E between its metallic plates has an interfacial charge $Q_0 = \epsilon_0 E$, where $\epsilon_0 = 10^{-7} / 4\pi c^2 = 8.854 \times 10^{-12}$ F/m is the dielectric permittivity of free space.

If the field E varies with temperature, the charge Q_0 follows exactly, there is no “inertia” in the vacuum response. If the capacitor is filled with a material medium-gaseous, liquid or solid-the charge induced is increased by the polarization P of the medium, so

$$Q = Q_0 + P = \epsilon_0 (1 + \chi) E = \epsilon E \quad (2.7)$$

Where ϵ is the permittivity and χ is the susceptibility of the dielectric medium. The dielectric constant ϵ_r of the sample was computed using the formula

$$\epsilon_r = C/C_0 \quad (2.8)$$

Where C is the measured capacitance and $C_0 = \epsilon_0 A/T$, where ϵ_0 is the permittivity of free space (8.854×10^{-12} F/m), A is area of the electrode and T is thickness of the sample.

Dissipation factor/tan δ

Dissipation factor is defined as the reciprocal of the ratio between the insulating materials capacitive reactance to its resistance at a specified frequency. The dielectric loss in an insulating materials can be described by the power dissipated per unit volume, called the specific loss, often, $\tan \delta$, in evaluating the degree to which a dielectric can dissipate the energy of the field; use is made of the angle dielectric loss and also the tangent of this angle.

The dielectric loss angle δ is the complement of the dielectric phase angle ϕ to 90° . The angle ϕ is the angular difference in phase between the voltage and current in the capacitive circuit. In the ideal case, the current phasor in such a circuit will lead the voltage phasor by 90° , and the loss angle δ will be zero. As the thermal dissipation of the electrical energy rises, the phase angle ϕ decreases, but the dielectric loss angle grows and so its function $\tan\delta$.

Two types of dielectric loss have been established for all polymers. The first type of dielectric loss, called dipole-segmental, is associated with orientational rotation of the polar units of the macromolecule under conditions where segmental movement is possible, i.e., in the high-elastic state (above the T_g of the polymer). The second type, called dipole-group, is due to orientation of the polar groups themselves. Losses of this kind may also occur below the T_g (glass transition temperature), i.e., in the high elastic state.

Resistance, Capacitance and Dielectric loss ($\tan \delta$) Measurement

We have used variable frequency digital LCR meter (General Radio, USA, model 1689/ Hewlett Packard, 4284 A/Soaltron 1260) to measure the electrical properties.

Four-probe method was used to measure resistance, capacitance and $\tan\delta$. The resistance, capacitance and $\tan\delta$ of the samples was measured by a constant voltage method. This technique results in a much more stable and reliable impedance measurement than the conventional constant current method. Electrical contact on the sample were made by applying an air drying type of silver paste, and then the sample was mounted between the two electrodes of the specially designed sample holder (as shown in Figure 2.5).

The a.c. electrical response of different samples was measured at ambient temperature. Resistance, Capacitance and $\tan\delta$ were measured as a function of frequency. The frequency was varied in a range from 50/100 Hz to 10 MHz for all the samples.

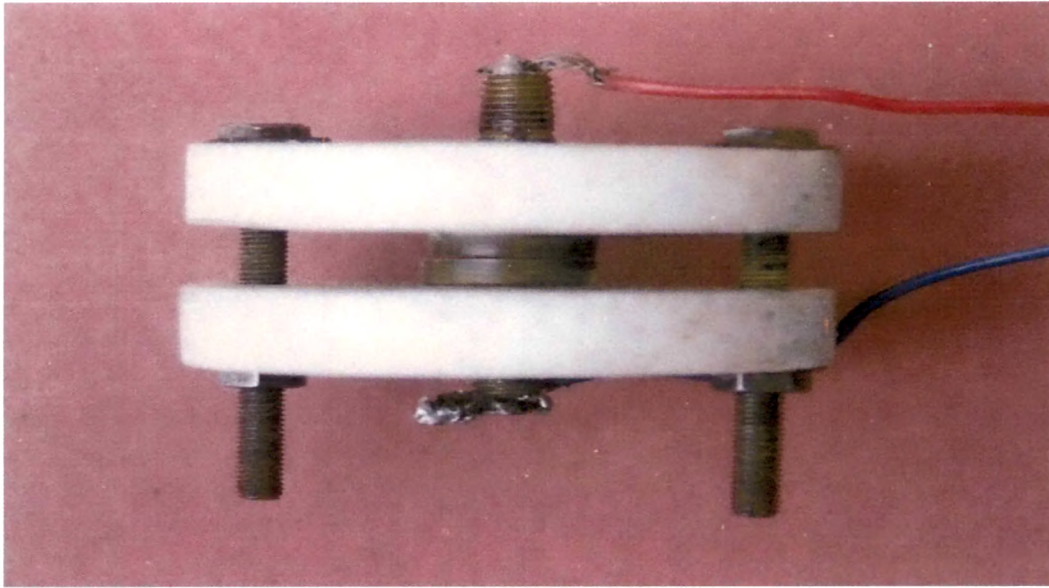


Figure 2.5 Sample Holder to measure electrical properties.

2.4.2 Vickers' Microhardness

Hardness is another important solid state property to characterize a material. Microhardness testing studies on crystals provide useful information concerning the lattice deformation resistance near the surface, anisotropy, evidence for structural multiphase in crystal as well as the other mechanical behaviour [12]. Study of the microhardness of undoped and doped crystals and the way in which this parameter is connected with dislocation density is of great interest for transducer applications involving mechanical vibrations [13, 14].

Hardness of a solid may be broadly defined as its ability to resist penetration by another harder solid. The ability of a material to resist permanent deformation is usually

considered as an interpretation of hardness [15]. The general definition of indentation hardness which is related to various forms of indenters is the ratio of applied load to the surface area of indentation. Thus hardness has the dimensions of stress. In fact, the chemical force in a crystal resists the motion of dislocations as it effectively involves the displacement of atoms. This resistance is the intrinsic hardness of a crystal. The hardness of a solid is as well defined by its resistance against lattice destruction and is considered to be a function of the interatomic forces [16, 17]. Attempts toward a physical definition of hardness were made by Friedrich [18], Goldschmidt [19] and others. Though the basic meaning of hardness remains the same i.e. a measure of resistance to plastic deformation, it has different meanings for different people: for metallurgist, it is resistance to penetration; for a lubrication engineer; it is resistance to wear; for a mineralogist, it is resistance to scratching, etc.

A lot of work on the hardness measurement in laboratory [20] has been carried out, ignoring search for a physical definition, although a workable definition has been developed and presented by Plendl and Gielisse [21] the determination of hardness of a material is normally made using a mechanical test that gives a measure of ease with which the material can be locally deformed. Hardness can be determined by various tests, such as scratch test, abrasion test, plowing test, rebound test, cutting test, damping test, erosion test and indentation test [20]. Most hardness testers produces plastic deformation in materials, and they all are based on microscopic indentations made using appropriate loads. The size of the impression of indentation is related to the applied load and the yield stress of the material [22].

Hardness defined as the ratio of load applied to the surface area of indentation, which for a Vickers' diamond pyramid indenter, is represented by the equation

$$H_v = 2P \sin \alpha / d^2 \quad (2.9)$$

where H_v is the Vickers' hardness number, P is the applied load in g, d in micrometer is the average diagonal length of the indentation mark and α is the angle between two opposite faces. With the particular geometry in our indenter, we use the formula

$$H_v = 1.854 \times P / d^2 \quad (2.10)$$

Where P is the in milliNewton (mN) and d in μm . The experimental error in H_v is computed by the relation [23],

$$H_v = 1.854 [(\Delta P / Y + P \Delta Y / Y^2)]^{1/2} \quad (2.11)$$

Where $Y = d^2$ and $\Delta Y = 2\Delta d$; ΔP , Δd being errors on P , Y and d respectively.

The Carl Zeiss Axiotech-Microscope along with its accessories used in the present work.

Vickers' Hardness Measurements

The method of indentation in hardness measurement is the most widely used method, primarily because it does not require large specimens and on a small specimen a number of measurements can be made. Indenters have been known to be either sharp or blunt according as their included angles are less or greater than 90° . As this angle increases, the indenter tends to be blunt and the influence of friction and prior strain hardening decreases.

The Vickers' diamond pyramidal indenter used in the present study has included angle of 136° which is a good compromise to minimize frictional effects and at the same time to give a well defined geometrical square to the indentation mark. The samples were mounted on a horizontal platform inserted in the collect of Vickers microhardness tester

which was attached to a metallurgical microscope (Fig. 2.6). The area for the indentation is selected by using bright field objectives. After selection of the area, an objective is replaced by Vickers' micro hardness indenter sensor from rotating nosepiece. Loads ranging from 100 mN to 1000 mN were used for making indentations, keeping the time of indentation constant as 30 seconds in all cases, (the diamond tip indents into the specimen at a pre-selected force gradient) since microhardness is observed to be independent of indentation time. The force is held constant for the duration of 30 seconds and then the diamond tip is automatically retracted to the resting position. To avoid surface effects, the distance between two consecutive indentations was kept more than three times the diagonal length of the indentation mark. The indented impressions were square shaped. The diagonal lengths of indentation marks were measured using a filar micrometer eyepiece at proper magnification and averages of these diagonal lengths were recorded. The Vickers' microhardness was calculated using the formula 2.10.

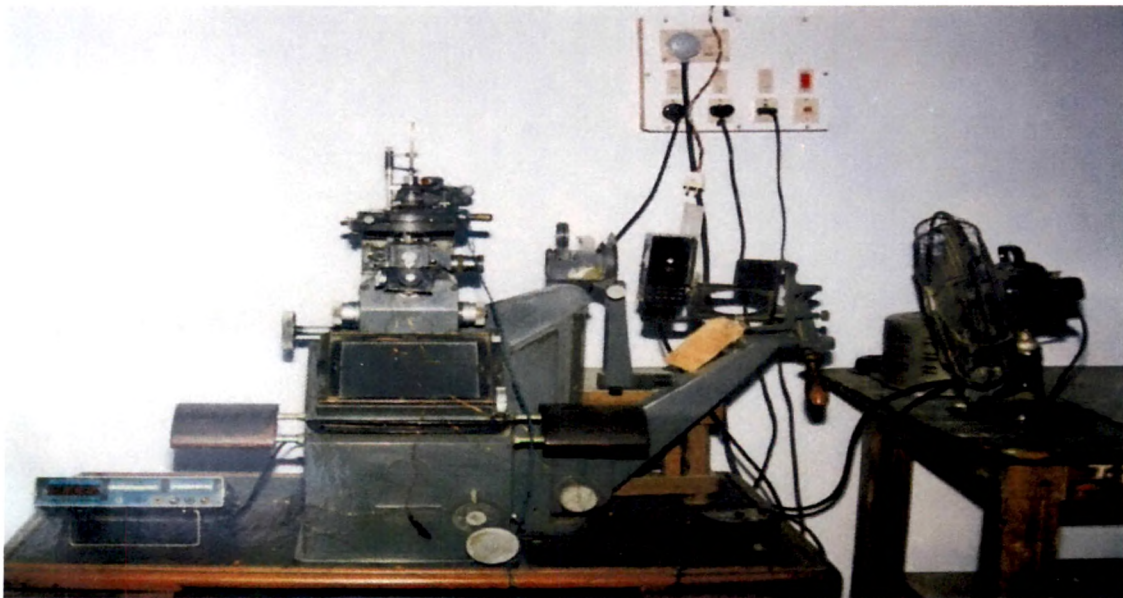


Figure 2.6 Vickers' Projection Microscope.

2.4.3 Atomic Force Microscopy (AFM)

The AFM was developed in 1986 by Gerd Binnig, Calvin Quate and Christoph Gerber in collaboration between IBM and Stanford University. In the fall of 1985 Gerd Binnig and Christoph Gerber used the cantilever to examine insulating surface. A small hook at the end of the cantilever was pressed against the surface while the sample was scanned beneath the tip. The force between tip and sample was measured by tracking the deflection of cantilever. This was done by monitoring the tunneling current to a second tip positioned above the cantilever. They could delineate lateral features as small as 300 \AA . The force microscope emerged in this way, In fact, without the breakthrough in tip manufacture, the AFM probably would have remained a curiosity in many research groups. It was Albrecht, a fresh student, who fabricated the first silicon micro cantilever and measured the atomic structure of boron nitride.

Today the tip-cantilever assembly typically is micro fabricated from Si or Si_3N_4 . The force between the tip and the sample surface is very small, usually less than 10^{-9} N . The detection system does not measure force directly. It senses the deflection of the micro cantilever. The detecting systems for monitoring the deflection fall into several categories. The device introduced by Binnig was a tunneling tip placed above the metalized surface of the cantilever. This is a sensitive system where a change in spacing of 1 \AA between tip and cantilever changes the tunneling current by an order of magnitude. It is straightforward to measure deflections smaller than 0.01 \AA . Subsequent systems were based on the optical techniques. The interferometer is the most sensitive of the optical methods, but it is somewhat more complicated than the beam-bounce method

which was introduced by Meyer and Amer [24]. The beam-bounce method is now widely used as a result of the excellent work by Alexander and colleagues.

In this system an optical beam is reflected from the mirrored surface on the back side of the cantilever onto a position-sensitive photodetector (see Fig. 2.7). In this arrangement a small deflection of the cantilever will tilt the reflected beam and change the position of beam on the photodetector [25]. A third optical system introduced by Sarid uses the cantilever as one of the mirrors in the cavity of a diode laser. Motion of the cantilever has a strong effect on the laser output, and this is exploited as a motion detector. According to the interaction of the tip and the sample surface, the AFM can be classified as repulsive or Contact mode and attractive or Non contact mode. Now the Tapping mode shows a prosperous future to image the micro-world.

Advantages of AFM

AFM can provide the following four main advantages in visualization.

- (a) Precision: The AFM can see structure at various length scales with ease and minimal sample preparation, from subnanometer to hundreds of micron.
- (b) High Resolution: It can be the surface with very high vertical resolution and provide detailed three-dimensional visualization.
- (c) Reduced Damage: The AFM can image samples in a relatively nondestructive manner.
- (d) Real-Time Monitoring: Changes in morphology as conditions are varied can be achieved in real-time.

Physics Behind AFM

The principles on how the AFM works are very simple. An automatically sharp tip is scanned over a surface with feedback mechanisms that enable the piezo-electric scanners to maintain the tip at a constant force (to obtain height information), or height (to obtain force information) above the sample surface (Fig. 2.8). Tips are typically made from Si_3N_4 or Si, and extended down from the end of a cantilever. The nanoscope AFM head employs an optical detection system in which the tip is attached to the underside of a reflective cantilever. A diode laser is focused onto the back of a reflective cantilever.

As the tip scans the surface of the sample, moving up and down with the contour of the surface, the laser beam is deflected off the attached cantilever into a dual element photodiode. The photodetector measures the difference in light intensities between the upper and lower photodetectors, and then converts to voltage.

Feedback from the photodiode difference signal, through software control from the computer, enables the tip to maintain either a constant force or constant height above the sample. In the constant force mode the piezo-electric transducer monitors real time height deviation. In the constant height mode the deflection force on the sample is recorded. The latter mode of operation requires calibration parameters of the scanning tip to be inserted in the sensitivity of the AFM head during force calibration of the microscope.

The primary purpose of these instruments is to quantitatively measure surface roughness with a nominal 5 nm lateral and 0.01nm vertical resolution on all types of

samples. Depending on the AFM design, scanners are used to translate either the sample under the cantilever or the cantilever over the sample is measured. Three dimensional topographical maps of the surface are then constructed by plotting the local sample height versus horizontal probe tip position.

The AFM images of pristine and irradiated samples were measured on 2x2, 5x5, and 10x10 μm^2 area of samples by III a Nanoscope Instrument at Inter University Consortium for Scientific Research (IUC-CSR) Indore and Inter University Accelerator (IUAC) New Delhi.

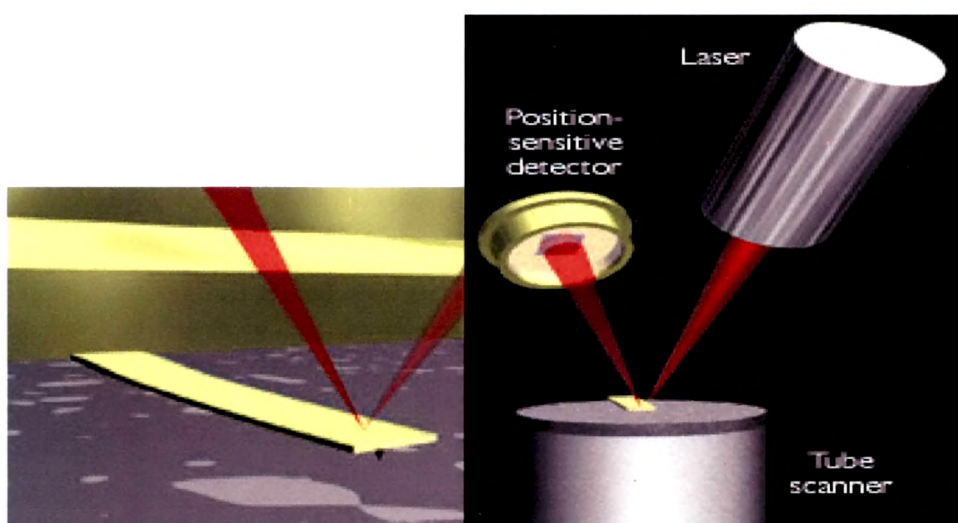


Figure 2.7 Concept of AFM and the optical lever: (left) a cantilever touching a sample; (right) the optical lever. Scale drawing; the tube scanner measures 24 mm in diameter, while the cantilever is 100 μm long.

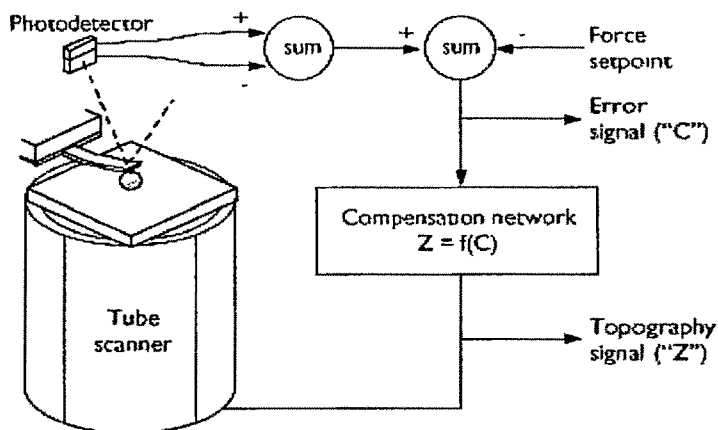


Figure 2.8 The AFM feedback loop. A compensation network (which in my AFM is a computer program) monitors the cantilever deflection and keeps it constant by adjusting the height of the sample (or cantilever).

2.4.4 Scanning Electron Microscopy (SEM)

The interactions of energetic electrons with the surface of a material provide the phenomena that is used for a number of analytical methods, particularly those which analyze near surface regions. A schematic diagram of a simple scanning electron microscope is shown in Fig. 2.9. There is a source of electrons, an accelerating electrode, a series of electron lenses to provide a very finely focused spot of electrons on the sample, the specimen, detectors, and the electronics necessary to image the signal of interest. This can be the specimen current, the back-scattered or secondary electrons, or a characteristic X-ray. The electron beam is focused to a fine spot the sample and the position of the spot on the sample is moved in a pattern called a raster. While the beam is also being moved in the same pattern (raster) as the electron beam on the sample. Thus , the picture on the cathode ray tube provides a very magnified image of the signal from the sample [26].

Insulating specimens in electron microscopes tend to charge under exposure to the electron beam. This causes distortion of the image and in many cases a reflection of the incident electrons from the highly charged surface. To overcome this effect, insulating samples are commonly coated with a thin layer of a conducting material to drain away this surface charge. Carbon is most commonly used for this purpose since it has a low atomic number and causes little interference with the image or with X-ray analysis. The backscattered and secondary electron images as well as the absorbed current images of a specimen in a scanning electron microscope are sensitive to surface morphology and compositional variations in the near surface region. This is the most common use for scanning electron microscopy on implanted insulators. Additionally, the use of energy dispersive X-ray analysis allows one to map the occurrence of various elemental species across the image area of interest.

SEM is used to get a phenomenological idea of what is happening to the surface of a material when the material is subjected to ion bombardment. The effects of sputtering or ablation or gas bubble formation can be detected. It is not a particularly useful method for quantitative measurements on ion bombarded samples. The scanning electron microscope (SEM) is a type of electron microscope capable of producing high resolution images of a sample surface. Due to the manner in which the image is created, SEM images have a characteristic three-dimensional appearance and are useful for judging the surface structure and surface morphology of the sample.

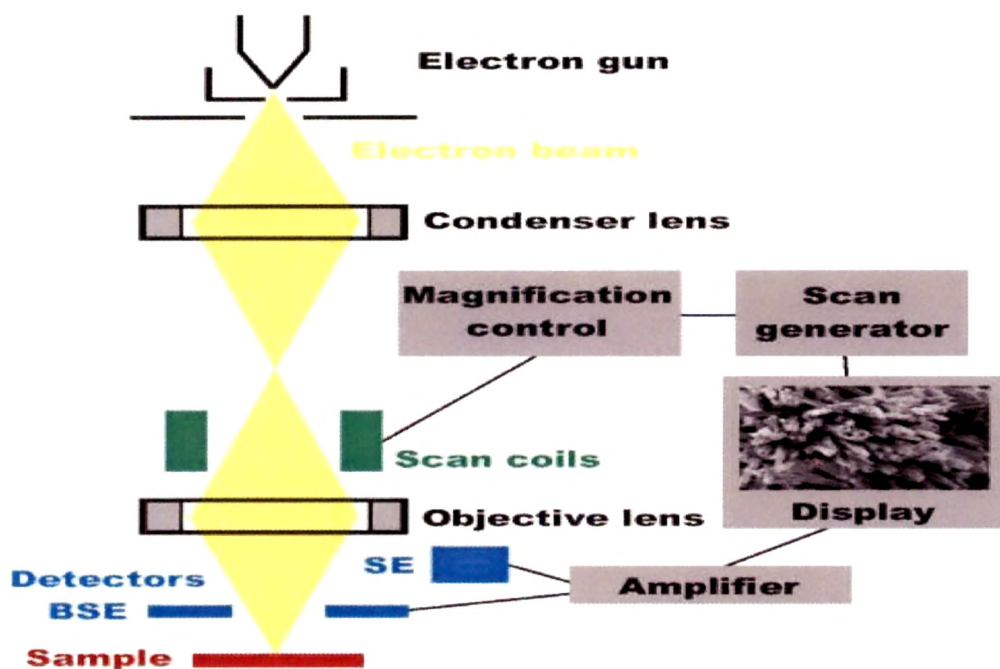


Figure 2.9 Schematic representation of a SEM.

The SEM images of pristine and irradiated samples were measured by Model:JEOL JSM 5600 instrument at Inter University Consortium for Scientific Research (IUC-CSR) Indore.

2.4.5 X-Ray Diffraction (XRD) Study

X-ray diffraction (XRD) is a complementary analytical technique to electron diffraction. One limitation of electron diffraction is small sample volume. If several electron diffraction patterns are not collected across the entire specimen, it is difficult to make a claim about the crystallinity of the bulk of the sample. X-ray diffraction, however, analyzes milligrams of sample (billions of particles in the 1 to 100 nm range)

while electron diffraction may analyse micrograms (thousands of particles in the 1 to 100 nm range).

An X-ray diffractometer utilizes some of the fundamental operations of a transmission electron microscope, so a useful analogy can be made. In X-ray diffractometer, X-rays are generated within an evacuated tube and exit through a window composed of a light element, usually beryllium. Inside the tube, a current is passed through a filament (usually tungsten) to generate electrons [27]. These electrons are then accelerated through a potential difference towards a metal target, such as copper. When the incoming electrons have sufficient energy to eject electrons from the core-shell (K shell) of copper, a characteristic spectrum is created (Fig. 2.10). The characteristic spectrum is composed of discrete energies, which occurs due to X-rays emitted by the 'falling in' of electrons to replace the ejected electron. Electrons 'falling in' from the L shell into the K shell give rise to copper K_{α} peaks, electrons from the M shell give K_{β} peaks and electrons from the N shell give K_{γ} peaks. K_{α} and K_{β} peaks are the most prominent peaks in the characteristic spectrum and since the K_{γ} peaks are a weak component they can be neglected. The K_{α} peaks and K_{β} peaks are doublets owing to the difference in energies of electrons 'falling in' from different L and M subshells respectively. Electrons will not 'fall in' from the L_1 subshell, but will fall in from the L_2 and L_3 subshells. Electrons that 'fall in' from the L_2 subshell give rise to K_{α_2} peaks and electrons that 'fall in' from the L_3 subshell give rise to K_{α_1} peaks. Due to the small difference in energy between the K_{α_2} and the K_{α_1} peaks, the K_{α} peak is a closely spaced doublet. A similar process occurs for electrons 'falling in' from two of the five M subshells to give a K_{β} doublet. For experiments where monochromatic radiation is

required, K_{α} radiation is of interest and a filter needs to be used to remove the K_{β} radiation [28]

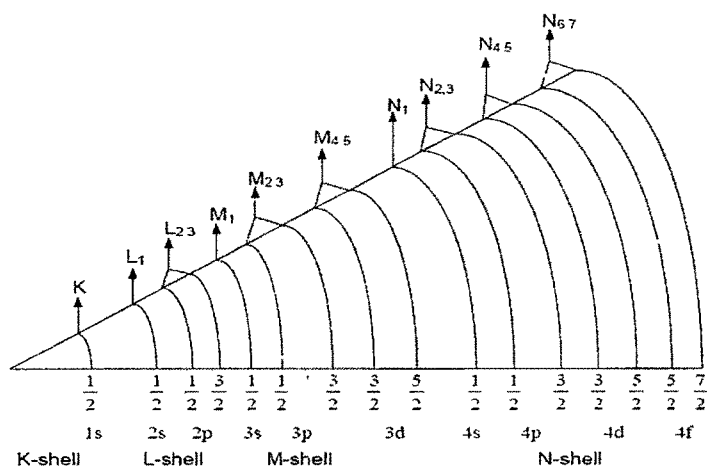


Figure 2.10 Schematic of electronic shells (29).

Diffraction of X-rays can be explained in a similar fashion to the diffraction of electrons. X-ray diffraction exploits the wave nature of electromagnetic radiation and as X-rays interact with a sample, they interfere with each other. Most of the X-rays undergo destructive interference; however, the X-rays that interact with the sample at a specific angle (θ_B) undergo constructive interference, which results in a signal for that particular angle. The angle θ_B is known as the Bragg angle and by using the formula

$$n\lambda = 2d_{hkl} \sin\theta_B \quad (2.12)$$

the interplanar d-spacings (d_{hkl}) can be calculated using a radiation source with known wavelength (λ). The d-spacings are similar commonly defined using the Miller index hkl notation.

To acquire a diffraction pattern, a sample placed onto a sample holder made of a material that has low x-ray absorption, e.g. an amorphous polymer like poly(carbonate). The sample holder is placed on a stage and is rotated within a range of angles between 0 and 158° [30]. The X-rays diffract from the sample and are collected at the detector. The diffraction pattern is then displayed on a computer where the peaks can be matched to a database of known crystal structures compiled by the JCPDS-International Center for Diffraction Data. Each peak has a value for 2θ , which is twice the Bragg angle. A given d-spacing corresponding to a lattice plane is obtained for each 2θ value. The size of crystallites in a system can be determined by using the Scherrer equation

$$L=K \lambda/b \text{ Cos}\theta \quad (2.13)$$

where L is the crystallite size, K is a constant that depends on the shape of the crystallites and b is the full width at half maximum of a diffraction peak and λ is the wavelength of the incident X-rays [31]. As crystallites decrease in size, their respective diffraction peaks broaden due to the increase in the number of lattice planes that diffract the incident x-rays. Crystallite size comparisons can be made by calculating the peak broadening for different sample. The XRD analysis was carried out using X-ray diffractometer with Cu-K α radiation ($\lambda=1.5418 \text{ \AA}$) XRD Bruker D8 Advance machine. The above formula is used in present work to calculate the crystallite size.

2.4.6 Fourier Transform Infra-Red (FTIR) Spectroscopy

Infraed spectroscopy is a characterization tool based on the interaction of electromagnetic radiation and chemical substance. It is one of the most powerful

analytical techniques which offer the possibility of chemical identification. One of the most important advantages of infrared spectroscopy over the other usual methods of structural analysis is that it provides useful information about the structure of molecules quickly, without lengthy evaluation methods.

The technique is based upon the simple fact that a chemical substance shows marked selective absorption in the infrared region. After absorption of IR radiations, the molecules of chemical substances vibrate at many rates of vibration, giving rise to close-packed absorption bands, called IR absorption spectrum which may extend over a wide wavelength range. Various bands will be present in IR spectrum which corresponds to the characteristic functional groups and bonds present in chemical substance. Thus, an IR spectrum of a substance is a fingerprint for identification.

The infrared region of electromagnetic spectrum covers a wide range of wavelengths from about 800 nm (end of visible region) to about 0.2 nm (beginning of the microwave region). The positions of bands in IR spectra are represented either in wave numbers (ν) or wave lengths (λ). The reciprocal centimeter has been referred to as 'Rydberg' and 'Kysner'. Band intensities in IR spectrum may be expressed either as transmittance (T) or absorbance (A). Transmittance is defined as the ratio of radiant power transmitted by a sample to the radiant power incident on the sample. On the other hand, absorbance is defined as the logarithm, to the base of 10, of the reciprocal of the transmittance,

i. e.
$$A = \log_{10} (1/T) \quad (2.14)$$

when a molecule absorbs radiation, its energy increases in proportion to the energy of the incident photon, and expresses by the relation.

$$\Delta E = h\nu = hc/\lambda \quad (2.15)$$

where h is the Planck's constant, λ is wavelength of radiation and c is the velocity of light.

Spectrometers may be either dispersive or non dispersive. In the former class are those instruments using gratings or prisms as the dispersing elements. Non dispersive type includes Fourier Transform Spectrometer. In the case of Fourier transform infrared (FTIR) spectrometers; although the final spectrum is the same as that produced on a dispersive spectrometer, the interferometer spectrometer operates on an entirely different principle. The basic optics are extremely simple. Such a device produces an interferogram which must be decoded to yield a spectrum. This process would seem to be an unnecessarily complicated way to obtain a spectrum, but the interferometer has important advantage in energy transmission over the dispersive spectrometer. FTIR spectrometer does not use slits. So the instrument is through putting the entire radiation beam at all times during scanning. The resolution depends only on the length of travel 'l' of the movable mirror and is equal to $(2l)^{-1}$. Thus for a 1 cm traverse the resolution is 0.5 cm^{-1} . For a 50 cm traverse (experimentally very difficult) the resolution would be 0.01 cm^{-1} . Moreover, the radiation is not dispersed in the interferometer; all of the source radiation (except that absorbed by the sample) is contributing to the signal at all times. Another advantage of the interferometer-computer combination is that the interferogram and resulting spectrum can be stored and manipulated within the computer [32].

The specifications of the instruments are listed below:

Source	Glowbar, high intensity and power stabilized
Wavenumber precession	0.0 cm ⁻¹ controlled with an internal He-Ne laser
Detector	High speed Deuterated Triglycine Sulfate (DTGD)
Resolution	4 cm ⁻¹ fixed
Beam Splitter	Proprietary ZnSe design
Wavenumber Range	6000 cm ⁻¹ to 510 cm ⁻¹

There is no routine adjustment to be made on the spectrometer.

The FTIR spectra of the pristine as well as irradiated samples of each polymer were recorded in transmission mode using Fourier transforming instrument (model 104-Bomem, Canada) keeping air as reference (Fig. 2.11). The measurements were done in the wave number range 4000-510 cm⁻¹ and the transmittance (or absorbance) spectra of the polymers were obtained (transmittance % or absorbance as a function of wavenumber). The variation of transmittance (%) for the pristine and irradiated polymers were compared and the peak analysis was done to study the disappearance of some existing bands, emergence of new ones and structural changes which includes the alteration in position and intensity of the characteristic bands with a resolution of 4 wave number.

The errors, while recording the spectra might be due to stray radiation, zero setting of the instrument, non continuous samples, atmospheric absorption, slit width, scan speed etc.



Figure 2.11 FTIR Spectroscopy set up.

2.4.7 Thermal Analysis

Thermogravimetric Analysis (TGA)

Thermogravimetric analysis is an analytical technique used to determine a material's thermal stability and its fraction of volatile components by monitoring the weight change that occurs as a specimen is heated. The measurement is normally carried out in air or in an inert atmosphere, such as Helium or Argon, and the weight is recorded as a function of increasing temperature. Sometimes, the measurement is performed in a lean oxygen atmosphere (1 to 5% O₂ in N₂ or He) to slow down oxidation.

TGA analysis is based on the principle of measurement of weight change associated with transition occurring due to rupture and/or formation of various physical and chemical bonds at elevated temperatures leading to the evolution of volatile products and formation of heavier reaction products.

TGA consists of a sensitive balance and a well controlled furnace or other suitable heating system to maintain a specified temperature. Data collected during a TGA experiment includes time, temperature and sample weight. The sample is placed in a platinum cell, which is then put on the sample pan, suspended in a quartz or alumina reaction tube, the atmosphere of which can be controlled. In the meantime, weights are placed on the weight pan to approximately balance the sample. When the weight of the sample changes upon heating, the beam held by taut band inclines. This inclination is detected by the photoconductive cell, and amplified. A current is allowed to flow through the feedback coil, placed in a uniform magnetic field, to produce a torque (electromagnetic force) to keep the beam horizontal. This is called the null method. Since the torque varies in proportion to the current, change of sample weight can exactly be measured by recording the current [33]

TGA is often used for studying degradation. Two aspects of degradation that are studied are thermal degradation and oxidative degradation of polymers. Thermal degradation is important because degradation that occurs during processing (such as extrusion) may be largely thermal and not oxidative. Polymers often degrade by the elimination of a hydrohalogen molecule, so the weight loss is directly related to the rate of polymer degradation. Oxidative degradation is also studied by TGA. In this study, the

weight loss profile is different from that for thermal degradation studies, but is more applicable to performance at high temperatures.

In the present study TGA was recorded by using a Universal V1.12E TA instrument in the presence of air from ambient temperature to 800⁰C at a predetermined heating rate of 20 ⁰C/min with air as the flushing gas.

Differential Scanning Calorimetry (DSC)

The Differential Scanning Calorimetry (DSC) is the fundamental technique of thermal analysis used to study and analyse the sample properties such as melting, glass transition, thermal history, crystallization, curing point, reaction kinetics and oxidative stability. It is also used to find specific heat, purity, polymorphism and chemical reaction measurements. The DSC instrument Universal V1.12E TA Instrument is used in present study, which is highly sensitive and allows the sensitive measurement of weight changes as small as few micrograms. Sketch diagram of DSC measurement is shown in Fig 2.12.

When an exothermic or endothermic change occurs in the sample material, power (energy) is applied or removed from the calorimeter. This amount of power involved is directly proportional to the energy change which measured and recorded. It is a unique method in the sense that it makes use of constantan discs as the primary means of heat transfer to the sample and references position as well as one element of the temperature measuring thermoelectric junctions. The cell temperature is controlled by using silver heating block, a resistance wound heater and closely coupled Platinel II control thermocouple. The block temperature is monitored by control thermocouple and appropriate amount of power is supplied to the heater as determined by the difference signal between thermocouple and the out put programmer. Heat from the block then

flows radially through the constantan disc towards the sample and reference platforms. Temperature at the raised sample and reference platform are monitored by chromel-constantan thermocouple formed by a junction of the constantan disc with a chromel wire at each platform position. The difference signal between these two thermocouple junctions is fed to the amplifier and which monitored on the Y-axis of the X-Y recorder. Variances in the sample property, energy absorption or release, weight or dimensional changes etc. are read on the Y or Y axis as a function of sample temperature on the X-axis of the recorder.

DSC measurements was carried out by a Universal V1.12TA instrument, calibrated through the melting points of indium and tin. About 6mg sample was heated in the calorimetric furnace in the temperature range of 40 °C-350 °C at a predetermined heating rate 10 °C/min.

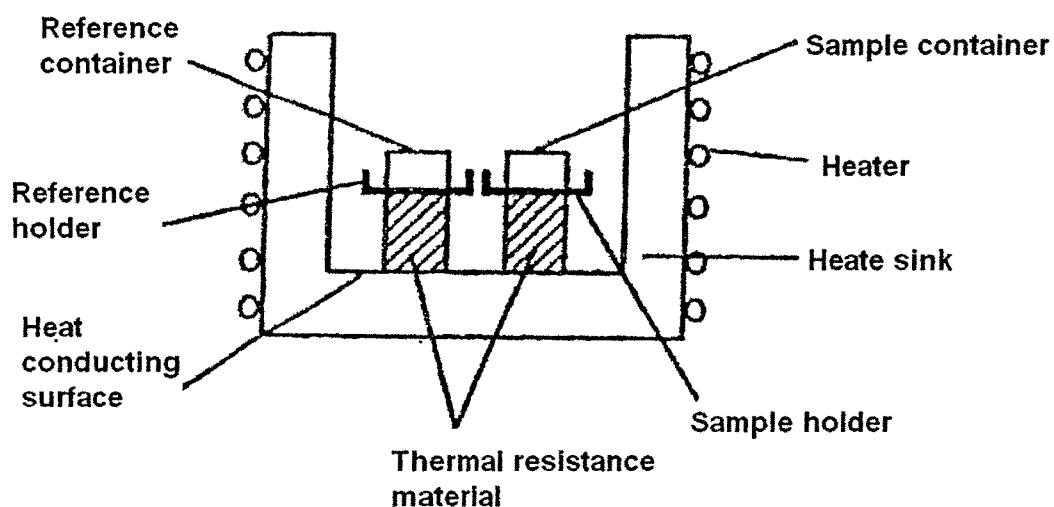


Figure 2.12 Sketch diagram of DSC measurement.

2.4.8 Mossbauer Spectroscopy

The interaction between a magnetic dipole or electric quadrupole moment of nucleus and a surrounding electromagnetic field lifts the degeneracy of the M states of nuclear level with spin I. The accompanying energy differences ΔE that characterizes the strength of surrounding field which induces splitting can be measured by various techniques. The techniques like ESR [34] and NMR [35] directly give the value of ΔE and PAC [36,37] operates in the time domain instead of energy domain and measures the precession frequency (ω). The measurement of nuclear spin precession frequency ω gives the information of energy difference as $\omega = \Delta E/h$. This technique makes use of coupling between γ ray emission probability and spin orientation. Mossbauer spectroscopy is the technique which makes use of nuclear resonance [38,39].

The Mossbauer Effect is based on the phenomena of recoilless emission and resonance absorption of γ rays [38]. It can provide local information about environment of particular atoms in solids, crystalline or amorphous materials. The concentration of the Mossbauer active atoms required to obtain useful spectrum is very low ($\approx 10^{14}$ to 10^{16} atoms cm^{-3}) as discussed by Williamson et. al. [40], hence very dilute systems are possible to study. This technique has an excellent energy resolution amongst all. Its energy resolution is $\sim 10^{-8}$ eV in 10^4 eV. It has numerous applications in Solid State Physics, Nuclear Physics, Geology, Chemistry, Biology, Medicine, Archeology etc.

Mossbauer spectrometer

There are two different methods of measuring the transmitted γ intensities.

- a) At constant velocity measuring the total number of transmitted photons for a fixed time.
- b) At constant acceleration the whole velocity range is scanned.

Mossbauer spectrometer usually operates in transmission geometry using a constant acceleration drive. In this geometry the source is vibrated whose velocity (V) linearly increases or decreases to Doppler modulate the gamma energy. The corresponding data of absorption in successive half periods of oscillations are stored with the help of multichannel analyzer in a Multi Scaling Mode (MCS). The switching of registered channel for data acquisition is synchronized with linearly changing speed of the source by a synchronization pulse.

Mossbauer spectrometer consists of following major parts as shown in Fig. 2.13

1. Mossbauer source and Absorber.
2. Drive Unit
3. Gamma ray detector
4. Data acquisition system

Mossbauer source and Absorber

a) Source

The source used was ^{57}Co in a rhodium matrix. Rhodium is a cubic and non magnetic metal which provides solid environment to ^{57}Co with high recoil free fraction. ^{57}Co has a half life 271.7 days and decays via electron capture to I=5/2 state of the ^{57}Fe . This daughter nucleus is in excited state and comes to its ground state by emitting three

different γ rays of 14.4KeV, 123 KeV and 137 KeV. The 14.4 KeV γ is transition corresponds to $3/2 \rightarrow 1/2$ levels. The mean life time of this $I=3/2$ state 97.8ns which corresponds to a natural line width of 0.194 mm/sec. For accurate measurement of the Mossbauer parameters, source should have line width corresponds to natural width. ^{57}Co in Rh matrix is one of the Mossbauer sources which have a high recoil free fraction and narrow line width. Decay scheme of the ^{57}Co is as shown in the Figure 2.14.

b) Absorber

Mossbauer absorbers used in the present study were dilute alloys of Germanium semiconductor. Natural abundance of ^{57}Fe in iron metal is 2% (i.e. 2×10^{13} Fe^{57} nuclei/gm mol). In order to get a good signal to noise ratio a minimum concentration of Mossbauer active atom is needed. The absorber samples in our study were made from 95% enriched iron 57 isotopes. The sample for Mossbauer study were taken in the powder form and spread uniformly in a 1.2 cm^2 area to make the absorbers.

Drive Unit

Drive unit of a function generator, Drive amplifier and a transducer. The source is mounted on a transducer which oscillates according to drive current from amplifier. The transducer is made up of moving coil in a constant magnetic field. Motion of the transducer excels induces current in sensing coil that is compared to reference current ramp. The difference (error) signal is feedback to drive current amplifier and consequently correction is done.

The reference current is triangular function of time with a linear rise from $-I_0$ to $+I_0$ with fly back to $-I_0$. The corresponding velocity is therefore triangular function of

time from $-V_0$ to V_0 . The maximum velocity imparted to the source is ± 25 mm/sec. The ramp generator circuit is triggered by synchronous signal from MCS.

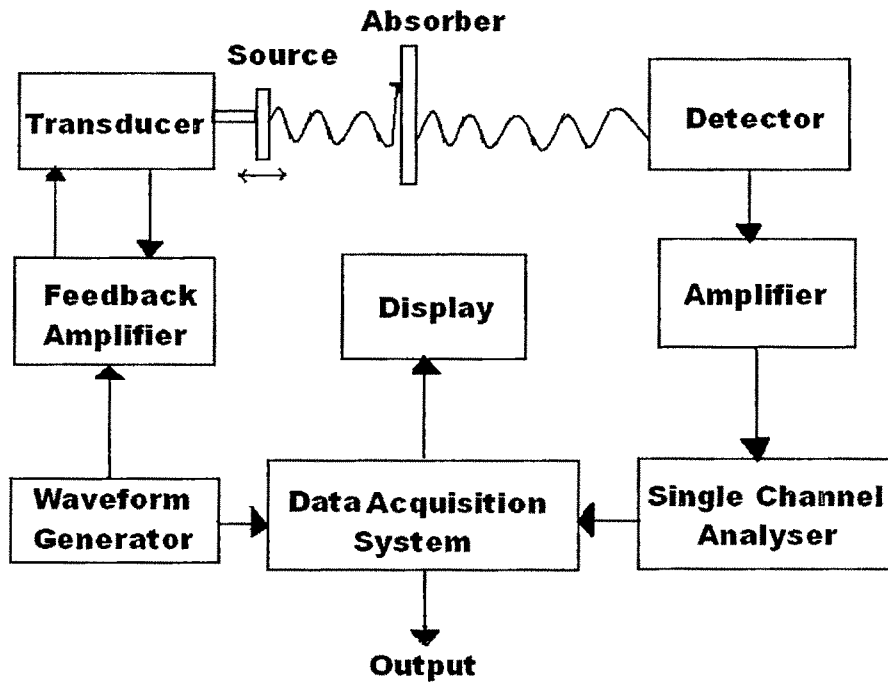


Figure 2.13 Shows the block diagram of Mossbauer Spectrometer

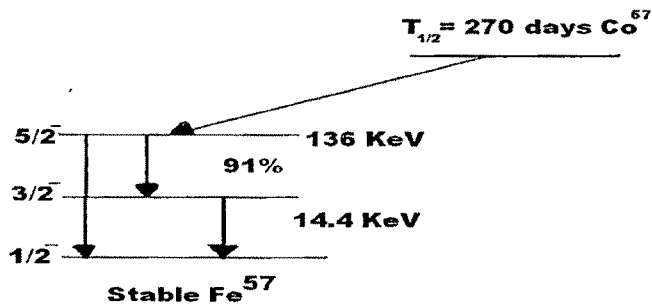


Figure 2.14 Decay Scheme of Co^{57}

Gamma ray detector and data acquisition systems

The detector used is a sealed proportional counter, filled with mixture of 90% Krypton and 10% methane gas. The applied bias voltage was around 2KV. Detector attached with pre-amplifier and a low-noise active filter amplifier, gives pulses of different voltage according to incident γ ray energy. The amplifier out put was fed to the Multi Channel Analyser (MCA). Energy selection for 14.4 KeV γ ray was done by a Single Channel Analyzer (SCA), lower level discriminator (LLD) and upper level discriminator (ULD) is set through software gating in a pulse height analysis (PHA) mode of MCA.

Gated pulses are converted into logic pulse in an Analog to Digital converter (ADC). The signals in the form of transmitted counts are accumulated in 1024 channels of MCA in a multi scaling mode synchronized with transducer acceleration. For one complete cycle of transducer oscillation two spectra can be recorded, one is for positive acceleration and other is for negative acceleration. As it operates in constant acceleration mode, time interval is constant for all velocity intervals hence each channel records the data for equal time duration. Synchronization of transducer and Multi Channel Analyzer are done by clock pulse generated by MCA. During the analysis full spectrum is folded around the centre point to produce single spectrum. Folding doubles the counts and flattens the background profile produced by the difference in intensity of source radiation.

References

- [1] Joel R. Fried, Polymer science and technology, Prentice Hall of India Private Limited, New Delhi (2000).
- [2] V. R. Gowariker, N. V. Viswanathan and Jaydev Sreedher, Polymer Science, New Age International (P) Ltd., Publishers, Edition (1996)1
- [3] D.W. Van Krevelen, Properties of polymers, 3rd ed., Elsevier, Amsterdam (1990).
- [4] E S Clerk, Polymeric materials, Metal Park, Ohio, USA (1974)
- [5] B.L Dickinson, Eng. Plast.4(1991) 297.
- [6] D. Kanjilal, S. Chopra, M. M. Narayanan, I. S. Iyear, V. Jha, R. Joshiand, S. K. Datta, Nucl. Instr. And Meth. A **328**(1993) 97.
- [7] R. G. Herb, Nucl. Instr. And Meth. **B 122** (1974)267.
- [8] D. K. Avasthi et al, ECASIA '93 Catania, Italy, Oct, 4-8,1993.
- [9] J. P. Biersack, J. F. Ziegler, code SRIM-2003, The stopping range of ions in matter (IBM Research), New York, USA(2003).
- [10] Dale and Malcolm, The radiation chemistry of macromolecules, Academic press, Vol. I (1972), Vol II (1973).
- [11] T. Murayama, Dynamic mechanical analysis of polymeric materials, Elsevier Amsterdam (1978).
- [12] H. Buckle, Mater. Rev. 4(1959)49.
- [13] A Sher, A. B. Chen and W. E. Spicer, Appl, Phys. Lett. **46**(1985)54.
- [14] C. Ascheron, C. Haase, G. Kuhn and H. Newmann, Cryst. Res. Techol. **26**(1989)K33.
- [15] N A. Ashby, N. Z. Engng **6** (1951)33.

- [16] C. W. Stillwell, *Crystal Chemistry*, Mc Graw-Hill Book Company, Inc., New York 29 (1938)p. 29 and 225-239.
- [17] H. Tertsch, *Festigkeitserscheinungen der Kristalle*, Springer-Verlag, Vienna (1949)171.
- [18] E. Friedrich, *Fortschritte der Chemie, Physik and Physikalischen Chemie*, Verlag Gebr.Bomtraeger, Berlin, Vol. 18 Heft 12 (1926)1-44.
- [19] V. M. Goldschmidt, *Geochemische Verteilungsgesetze der Elemente*, Jacob Dybwad-Verlag, Oslo (1927) 102-127.
- [20] B. W. Mott, *Microindentation Hardness, Testing*, Bitterworths, London (1966)9.
- [21] J. N. Plendl and P. J. Gielisse, *Phys. Rev.***125** (1962) 828.
- [22] D. J. Clinton and R. Morrell, *Mater. Chem. Phys.* **17**(1987)461.
- [23] P. N. Kotru, A. K. Razdan, B. M. Wanklyn, *J. Mater. Sci.* **24** (1989) 793.
- [24] G. Meyer, N. N. Amer, *Appl. Phys. Lett.* **53** (1988)1045.
- [25] Source:<http://stm2.nrl.navy.mil/how-afm.html//General%20concept>.
- [26] D. J. Clinton and R. Morrell, *Mater. Chem. Phys.* **17**(1987)461.
- [27] D. Halliday, R. Resnick, J. Walker, *Fundamentals of physics: Extended*, 5th ed., John Wiley & Sons, Inc., New York (1997).
- [28] E. W. Nuffield, *X-ray Diffraction Methods*, John Wiley & Sons, Inc., New York, (1966).
- [29] D. B. Williams, C. B. Carter, *Transmission electron microscopy: A Textbook for Materials Science*, Vol. 4, Plenum Press, New York (1996).

- [30] "Technical Data of D-500," in Technical University Muenchen,
http://www1.physik.tu-muenchen.de/lehrstuehle/E21/x_ray_la
 b/D500/parameters.html, April 02, 2005.
- [31] A. Guinier, X-ray Diffraction: In Crystals, Imperfect crystals and amorphous
 bodies, W. H. Freeman and Company, San Francisco (1963).
- [32] P. J Flory and D. Y. Yoon, Nature **222** (1978) 226.
- [33] L. C. Martin, The theory of the microscope. Blackie, London, (1966).
- [34] K. A. McLauchlan, Magnetic resonance, Clarendon Press, Oxford (1972).
- [35] H. Ackermann, D. Dubbers and H. J. Stockmann, Adv. nucl. quadrupole
 resonance, Vol III, ed. J. A. S. Smith , Heyden London (1978) 66.
- [36] Frauenfelder and R. M. Steffen, in: Alpha, Beta, Gamma ray spectroscopy, Vol. 2,
 ed. K. Sieghban ,North Holland, Amsterdam (1965) 997.
- [37] W. D. Hamilton, The electromagnetic interaction in nuclear spectroscopy, North
 Holland, Amsterdam (1975).
- [38] G. K. Werthiem, Mossbauer effect, Academic Press, London (1964).
- [39] N. N. Greenwood, and T. C. Gibbs, Mossbauer spectroscopy, Chapman and Hall
 Ltd., London (1971)19.
- [40] D. L. Williamson, L. Niesen G. Weyer, R. Sielemann, G. Langouche, Hyperfine
 interaction of defects in semiconductors, ed. By Elsevier publisher, Netherlands
 (1992).